THE GEMINI SPECTRAL LIBRARY OF NEAR-IR LATE-TYPE STELLAR TEMPLATES AND ITS APPLICATION FOR VELOCITY DISPERSION MEASUREMENTS*

Cláudia Winge[1], Rogemar A. Riffel[2], and Thaisa Storchi-Bergmann[2]
[1] Gemini Observatory, c/o Aura, Inc., Casilla 603, La Serena, Chile; cwinge@gemini.edu
[2] Universidade Federal do Rio Grande do Sul, IF, CP 15051, Porto Alegre 91501-970, RS, Brazil

ABSTRACT

We present a spectroscopic library of late spectral type stellar templates in the near-IR range 2.15–2.42 μm, at $R = 5300$–5900 resolution, oriented to support stellar kinematics studies in external galaxies, such as the direct determination of the masses of supermassive black holes in nearby active (or non-active) galaxies. The combination of high spectral resolution and state-of-the-art instrumentation available in 8 m class telescopes has made the analysis of circumnuclear stellar kinematics using the near-IR CO band heads one of the most used techniques for such studies, and this library aims to provide the supporting data sets required by the higher spectral resolution and larger spectral coverage currently achieved with modern near-IR spectrographs. Examples of the application for kinematical analysis are given for data obtained with two Gemini instruments, but the templates can be easily adjusted for use with other near-IR spectrographs at similar or lower resolution. The example data sets are also used to revisit the "template mismatch" effect and the dependence of the velocity dispersion values obtained from the fitting process with the characteristics of the stellar templates. The library is available in electronic form from the Gemini Web pages.

Key words: astronomical data bases: miscellaneous – methods: data analysis – stars: late-type – techniques: spectroscopic

1. INTRODUCTION

Spectral templates, usually late-type stars, are required for the analysis of kinematical data on external galaxies or other stellar ensembles (e.g., Emsellem et al. 2001; Márquez et al. 2003; Barbosa et al. 2006; Ganda et al. 2006; Cappellari et al. 2007; Dumas et al. 2007; Riffel et al. 2008; Cappellari et al. 2009; Riffel et al. 2009). In the near-infrared (hereafter near-IR), the most commonly used features are the CO overtone bands at $\lambda > 2.29$ μm. These band heads originate from evolved stars and are the strongest features in the 1–3 μm spectral range of stellar systems. The features are deep and sharp, and at least the first two overtones are located in regions of the IR spectrum relatively clean from telluric lines.

Although observational and theoretical libraries exist at lower spectral resolutions ($R \leqslant 3000$; e.g., Kleinmann & Hall 1986; Wallace & Hinkle 1997; Ramirez et al. 1997; Förster Schreiber 2000; Ivanov et al. 2004), no comprehensive set of stellar kinematic templates was available for use with the $R \sim 6000$ configuration of the two Gemini NIR instruments used for stellar population kinematic studies in external galaxies, the Near-infrared Integral Field Spectrograph (NIFS) and the Gemini Near-Infrared Spectrograph (GNIRS) with the 111 line mm^{-1} grating (both long-slit and Integral Field Unit—IFU), and, therefore, all observing programs using those configurations would invariably spend some science time taking a small set of stellar spectra to use as templates. This led to a constant multiplication of data taking, since those targets were defined as program calibrations and were not made available to other users until the end of the default 18-month proprietary period.

During semester 2006B at Gemini South, given the unusually poor conditions over the whole semester, a Director's Discretionary "poor weather" program was specifically carried out to provide the NIR community with a larger set of late (F7–M3 types) stellar spectra in the range 2.24–2.43 μm, including the

four CO overtone bands, at $R \sim 5900$ resolution. Most of the targets were also observed at a slightly bluer spectral range (2.15–2.33 μm) to improve usefulness for NIFS users, overlapping with the red setting on the first two CO bands.

To the original sample of 29 stars observed with GNIRS, another 11 were added from NIFS observations obtained as part of programs GN-2006A-SV-123, GN-2006B-Q-107, and GN-2007A-Q-25, covering the full range 2.1–2.5 μm at a similar resolution to that of the GNIRS data.

2. OBSERVATIONS AND DATA REDUCTION

2.1. The GNIRS Data

GNIRS (Elias et al. 1998) is a multi-configuration spectrograph originally deployed at Gemini South, now moved to Gemini North, that allows for several combinations of resolution and wavelength coverage. The two modes most commonly used for the science relevant here were the long-slit with the 32 line mm^{-1} or 111 line mm^{-1} gratings, which yield resolutions of up to $R \sim 2000$ and $R \sim 6000$, respectively (depending on the slit used), and the Integral Field Unit with the same gratings, where the internal optics projected each 0."15 slice into two detector pixels in the dispersion direction, resulting in a single fixed resolution similar to the one obtained with the 0."3 long-slit, and a field of view of 3."2 × 4."8. The IFU has been decommissioned at Gemini North, given the capability overlap with NIFS.

The observed sample was selected from a list kindly provided by G. Doppmann, compiled from the literature (mostly based in Cayrel de Strobel et al. 1997), and the selection was based exclusively on observability: targets that were visible for as long as possible during the semester, bright enough to provide the desired S/N on a reasonable on-source time under cloudy, poor seeing conditions, and having a hot (A0–A7) star close enough—and bright enough—to be used for telluric correction. In addition, both target and telluric stars had to have

Table 1
GNIRS Sample

Object	Mag	Sp Type	T_{eff}	log g	Blue Setting (2.15–2.33 μm)		Red Setting (2.24–2.43 μm)	
	(V)		(K)		Date	Res. (Å)	Date	Res. (Å)
HD 20038	8.91	F7 IIIw	5196	2.62	2006 Oct 13	2.97	2006 Sep 12	2.76
					2006 Oct 18		2006 Oct 7	
							2006 Oct 13	
HD 209750	2.90	G2 Ib	5091	1.45	. . .	. . .	2006 Oct 20	2.99
HD 6461	7.65	G3 V	5110	2.30	2006 Oct 10	2.98	2006 Sep 5	2.93
							2006 Oct 7	
HD 173764	4.23	G4 IIa	4700	0.94	2006 Oct 12	3.02	2006 Sep 4	2.89
							2006 Oct 21	
HD 36079	2.84	G5 II	5170	2.27	2007 Jan 4	3.16	2006 Sep 14	3.02
HD 1737	5.17	G5 III	4790	3.05	2006 Oct 8	2.93	2006 Sep 14	3.02
HD 213789	5.89	G6 III	4820	2.88	. . .	. . .	2006 Sep 4	2.89
HD 212320	5.92	G6 III	4790	2.87	2006 Oct 6	2.94	2006 Sep 4	2.89
HD 213009	3.97	G7 III	4800	2.0	. . .	. . .	2006 Sep 3	3.10
HD 35369	4.14	G8 III	4880	2.76	2006 Oct 15	2.96	2006 Oct 5	2.88
HD 64606	7.44	G8 V	5040	4.0	2007 Jan 4	3.16	2007 Jan 2	2.79
HD 224533	4.89	G9 III	4960	3.19	2007 Jan 7	2.79	2006 Sep 14	3.02
HD 4188	4.78	K0 III	4755	2.90	2006 Oct 12	3.02	2006 Oct 5	2.88
HD 206067	5.11	K0 III	4740	2.73	2006 Oct 6	2.94	2006 Aug 31	2.99
HD 34642	4.83	K0 IV	4730	3.39	2006 Oct 17	2.89	2006 Sep 12	2.71
HD 198700	3.66	K1 II	4383	0.80	. . .	. . .	2006 Sep 4	2.89
							2006 Oct 21	
HD 218594	3.66	K1 III	4430	2.34	2006 Oct 20	2.93	2006 Sep 3	3.10
HD 26965	4.41	K1 V(a)	5091	4.31	2006 Dec 12	3.07	2006 Sep 13	3.01
							2006 Oct 1	
HD 39425	3.12	K2 III	4582	2.80	2006 Dec 12	3.07	2006 Oct 1	3.01
HD 38392	6.15	K2 V	4990	4.50	2006 Oct 17	2.89	2006 Oct 1	3.01
HD 4730	5.61	K3 III	4220	2.10	2006 Oct 8	2.93	2006 Sep 3	3.10
HD 191408	5.31	K3 V	4893	4.55	. . .	. . .	2006 Sep 5	3.01
							2006 Oct 1	
HD 9138	4.84	K4 III	4040	1.91	2006 Oct 19	2.97	2006 Sep 10	2.94
HD 720	5.42	K5 III	4160	2.02	2006 Oct 12	3.02	2006 Sep 10	2.94
HD 32440[a]	5.47	K6 III	. . .	. . .	2007 Jan 6	2.79	2007 Jan 4	2.73
HD 63425B[a]	7.71	K7 III	. . .	. . .	2006 Dec 12	3.07	2006 Dec 12	2.75
HD 113538[a,b]	9.02	K8 V	. . .	. . .	2007 Jan 4	3.16	2007 Jan 6	2.90
HD 2490	5.43	M0 III	3652	4.0	2006 Oct 15	2.96	2006 Sep 11	2.95
HD 112300	3.38	M3 III	3652	1.3	. . .	. . .	2007 Jan 16	2.89

Notes. The spectral resolution in columns (7) and (9) has been measured from the Ar arc lines. For those stars observed in more than one night, the value given is the resulting resolution for the combined spectrum.
[a] Not in the Cayrel de Strobel et al. (1997) list; magnitude and spectral type from Simbad.
[b] In Figure 3, this star falls quite off the overall trend of EW with T_{eff}. The spectral type quoted here is from older references. Gray et al. (2006) give it a K9V spectral type (thus moving the point further to the left), but also indicate presence of (minor) chromospheric activity in this star. The spectrum is shown in Figure 1(f).

a bright ($V < 13$ mag) star available in the guide probe patrol field.

The observations were done using the IFU (Allington-Smith et al. 2006, 2007) with the 111 line mm^{-1} grating, yielding a resolving power of $R \sim 5900$. The list of observations is given in Table 1, where for each object are listed the V magnitude, effective temperature and surface gravity when available, as well as the observing dates and the spectral resolution, measured from the arc lines, for the "blue" (centered at 2.245 μm) and "red" (centered at 2.335 μm) settings, respectively.

The observing conditions also determined the instrument configuration: to achieve $R = 5900$ with GNIRS in long slit mode, one would have to use the 0$''$.30 slit, implying very large slit losses under poor seeing conditions (FWHM $> 0''.80$ in K). Given the superior GNIRS IFU performance in the K band (over 90% of that of the equivalent long slit mode), there was only a small loss in sensitivity by using the IFU+111 line mm^{-1} grating configuration.

The standard group of observations included a science target, one telluric standard star, a set of calibrations comprising three arcs, and a set of ten QH lamp flats. Calibrations (arcs and flats) were usually observed right after the science target, or after a set of targets was observed, but before the grating was moved to another configuration.

Observing sequences were defined as several (2–5) repeats of ABBA sequences, with a 4$''$ offset between the A (object) and B (sky) positions in a direction perpendicular to the long axis of the IFU field-of-view, large enough to move a centered object completely off to sky. On-target efficiency with this setup gets reduced by 50%, but it avoids the problem of overlapping point-spread function wings due to the small size of the IFU if trying to dither on source.

The GNIRS data frames as delivered to the Gemini Science Archive are in the standard Gemini MEF (Multi-Extension Format), where the primary header unit (PHU, extension [0]) includes all header information from telescope, environmental

monitoring system and instrument, and the data extension [1] contains the pixel values. Data reduction was performed using the tasks in the *gemini.gnirs* IRAF package,[3] release Version 1.9, of 2006 July 28 and comprised the following steps:

For the calibrations (flats and arcs):

1. *nsprepare*: this task reformats the data files to add the IFU Mask Definition File (MDF), which contains the information on the position of the individual slices in detector coordinates, and applies the linearity correction to the pixel data. The resulting file contains the PHU, one binary table extension with the MDF, and one data extension with the actual pixel values.
2. *nsreduce*: cuts out each of the 21 IFU slices according to the MDF inserted above to a separate data extension. No dark correction was applied to either flats or arcs.
3. *nsflat*: combines the ten frames by data extension, using *ccdclipping* for rejection and normalizing by the median of the illuminated area in each slice, as defined in the MDF. On average, the processing resulted in a S/N ~ 200–300 for each extension, with exception of slices 1 and 21 (which were partly vignetted) and slice 13 (which was damaged).
4. used *gemcombine* to average the three processed arc frames to improve visibility of faint lines, then *nswavelength* to obtain the wavelength solution from the combined arc. For the standard Gemini Ar lamp, there were four lines in the "red" setting, and six in the "blue" setting. A low-order polynomial (legendre order = 3) was used for the fitting, with residuals of the order of 0.15 Å or less.

For the science data and telluric stars:

1. *nsprepare*: same as for the calibrations.
2. *nsreduce*: after cutting the individual slices to separate data extensions, the task corrects the frames for the flat-field, and subtracts adjacent object-sky frames.
3. *nsstack*: since we had only one position with actual data (the B position was blank sky), and the targets were all bright point sources observed under poor seeing conditions, we simply stacked all A positions without any effort to improve alignment of the individual frames by shifting according to the offsets registered in the headers. In most cases all frames were within 0″.3 tolerance, but there were a few observations where drifts of up to 0″.8 were seen, usually due to clouds or very poor seeing affecting the guiding performance.
4. *nstransform*: the wavelength transformation is applied to the stacked frame.
5. *nsextract*: finally, we interactively extracted the spectrum from each slice, in order to exclude those with very low signal, since the targets were not always well centered in the IFU field-of-view, the two edge slices, and the damaged slice when the spectrum happened to fall within the damaged region. The output from this task is still an MEF file, with each data extension containing a one-dimensional spectrum.
6. used a simple IRAF cl script wrapped around *specred.scombine* to combine all valid spectra obtained in the previous step. At this point, a single one-dimensional standard FITS spectrum is created, but most of the information contained in the PHU of the MEF files is lost, as *scombine* propagates the header of the first extension included in the combining list, ignoring the content of the PHU.

Table 2
NIFS Sample

Object	Mag (V)	Sp Type	Date	λ_c (μm)	Resolution (Å)
HD 210885	7.28	G8 II	2007 Oct 15	2.25	3.17
HD 107467	7.37	G8 III	2006 Jan 18	2.20	3.20
HD 105028	7.37	K0 III	2007 Apr 30	2.20	3.14
BD +44337	8.56	K5 Ib	2006 Dec 30	2.25	3.22
HD 10598	8.31	K2 III	2006 Dec 30	2.25	3.22
HD 109655	7.07	K5 III	2006 Jan 1	2.20	3.12
HD 3989	7.31	K5 II	2007 Oct 15	2.25	3.17
HD 30354	8.47	M2 III	2007 Jan 30	2.25	3.26
HD 236791	8.91	M3 III	2007 Jan 2	2.25	3.23
HD 27796	7.75	M3 III	2006 Dec 30	2.25	3.22
HD 235774	8.69	M5 III	2007 Oct 15	2.25	3.17

7. finally, applied the telluric correction in the science data, using the standard *specred.telluric* task, and combined all spectra for those targets observed in different nights.
8. added back the header information lost in step 6, corresponding to the content of the PHU of the MEF frame obtained in step 5. This preserves all telescope, instrument, and program information.
9. removed the continuum shape by fitting a low-order polynomial to the final one-dimensional spectrum, and corrected all spectra to rest velocity, by measuring the central wavelength of a strong, isolated line (Mg I at 2.2814 μm) and using it as a reference zero point for all data sets. This corrected in a single step the intrinsic radial velocity and any zero-point offset that could exist from the wavelength calibration.

Figures 1(a)–(f) show the resulting spectra, with "red" and "blue" settings combined when it applies.

2.2. The NIFS Data

NIFS (McGregor et al. 2003) is an IFU spectrograph with coronographic masks, optimized for use with the Gemini North Adaptive Optics (AO) system Altair. In the *K* band, the standard NIFS configuration yields a 2 pixel spectral resolution of $R = 5290$ (at 2.2 μm), covering the entire 1.99–2.40 μm range in a single setting.

The data were obtained either as program calibrations for GN-2006A-SV-123 and GN-2007A-Q-25, and therefore based solely in observability and brightness, or as part of a "poor weather" program GN-2006B-Q-107, and in this case following the same rationale as the GNIRS sample (bright enough for poor conditions, with proper telluric and guide stars available). The stars observed as part of 06A-SV-123 and 07A-Q-25 used the AO wavefront sensor for guiding, while for 06B-Q-107, the AO fold was parked and guiding was done using the peripheral wavefront sensor only (no AO correction).

The selected instrument configuration was the K_G5605 grating and HK_G0603 filter, resulting in an FWHM for the arc lamp lines of 3.2 Å. Each observation consisted of five individual exposures, with the star centered on the array then offset to each corner. Table 2 lists the observations, where for each object we present the spectral type, observing date(s), spectrum central wavelength (in μm), and spectral resolution from the arc lines (in Å).

The data reduction was done in a similar way as for the GNIRS data, using the corresponding tasks in the *gemini.nifs* IRAF package. The reduction procedure included trimming
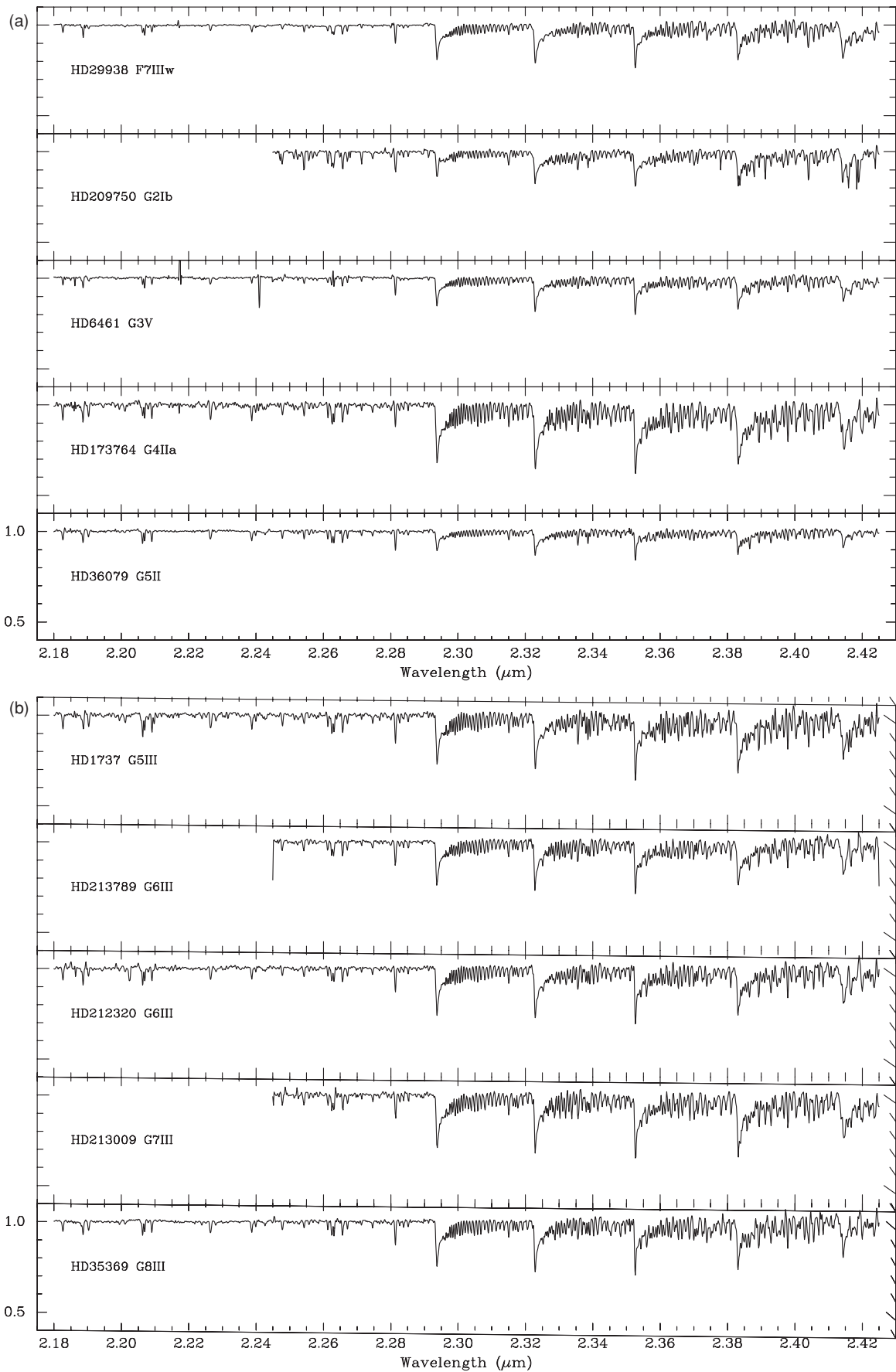
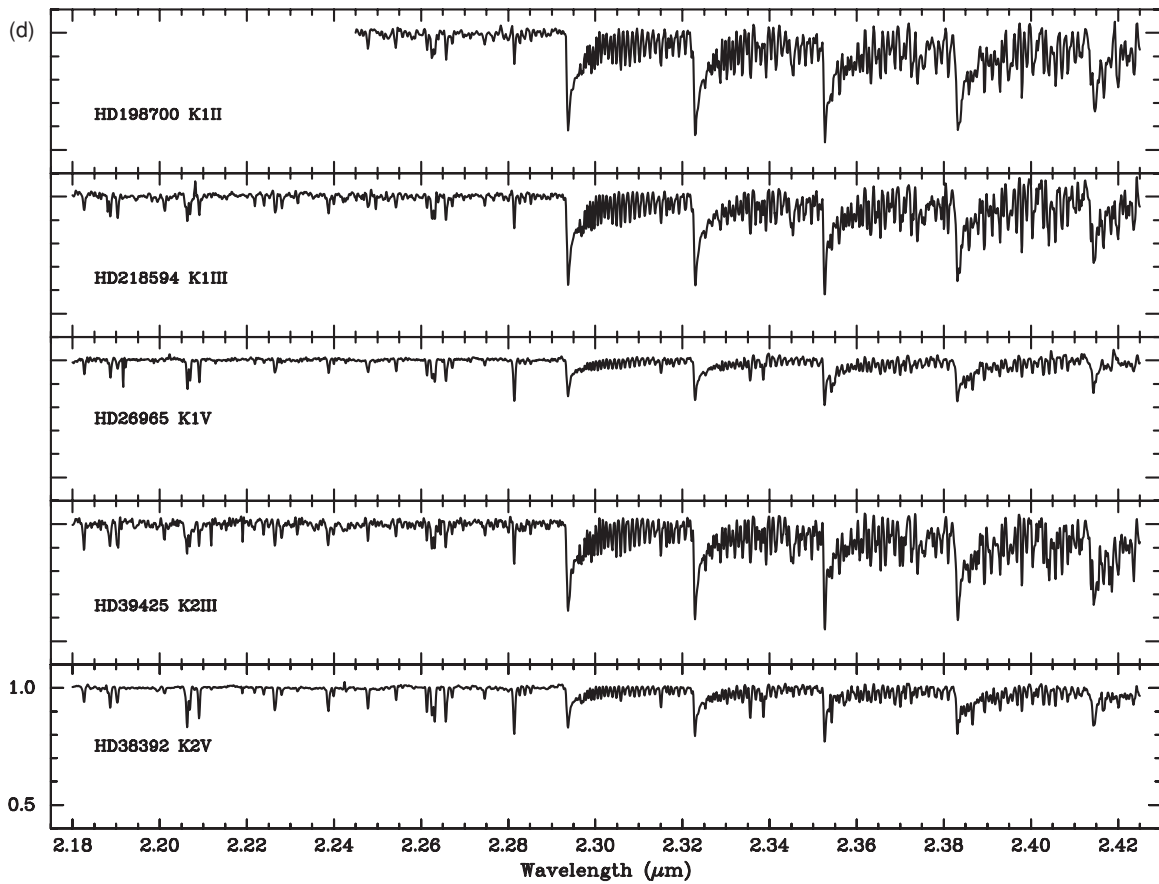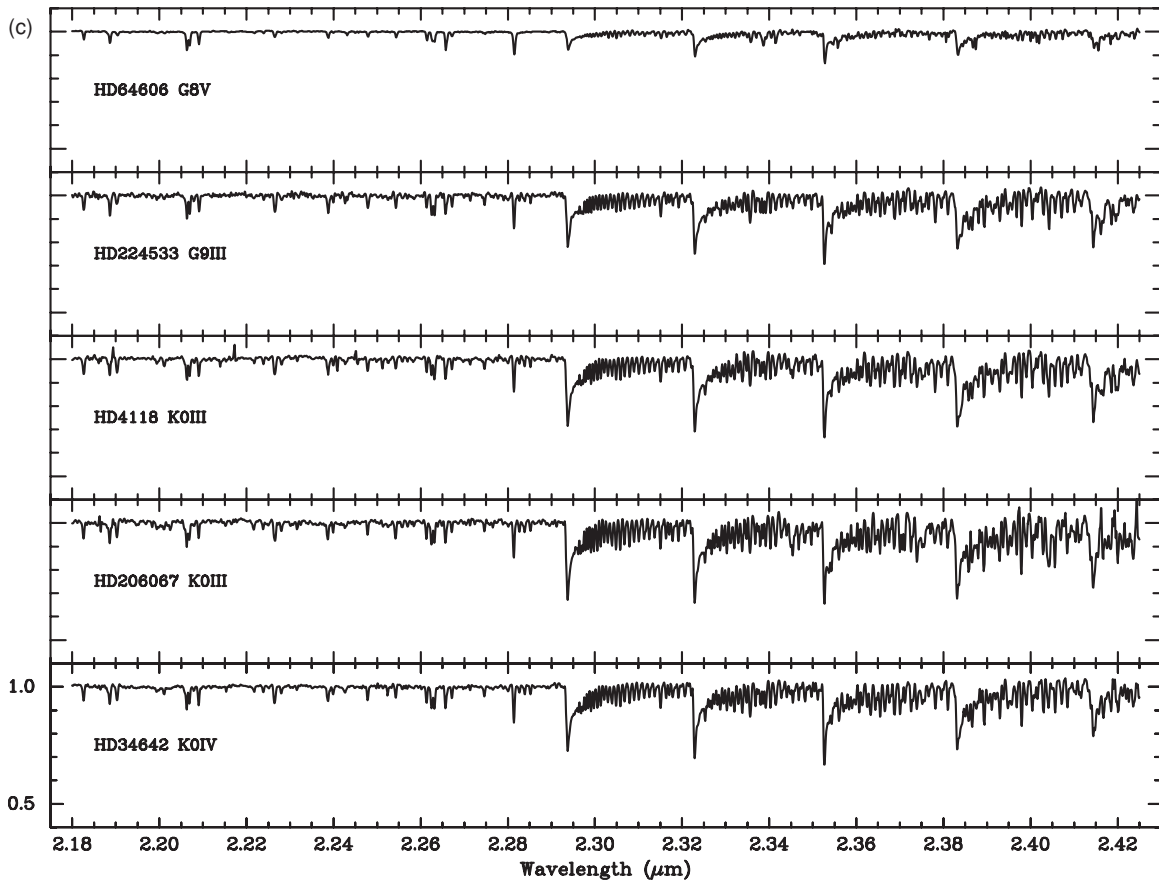**Figure 1.** GNIRS template spectra, arranged by spectral type.
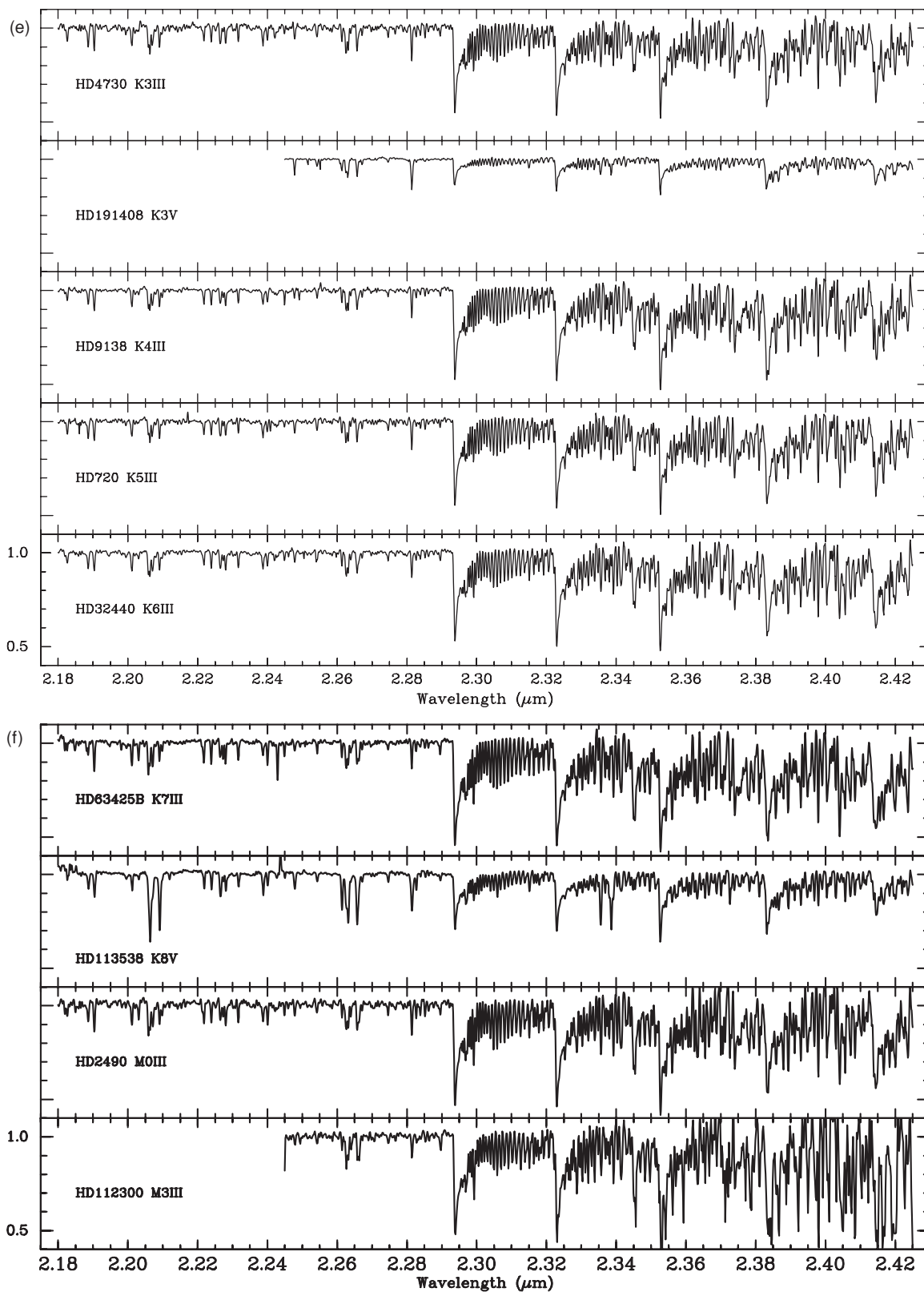
Figure 1. (Continued)

Figure 1. (Continued)

the images, flat-fielding, sky subtraction, wavelength, and s-distortion calibrations. Removal of the telluric bands and flux calibration was executed in a single step by interpolating a black body function to the spectrum of the telluric standard star. Finally, the continuum shape was removed from the spectrum of each star (using the IRAF task *continuum*), normalizing the continuum fluxes to unity.

Similar to the GNIRS spectra, the extraction procedure results in loss of the primary header content. This was added back to the spectra in order to propagate the relevant instrument/

telescope information. The spectra were also shifted to a common reference point using the same Mg I line. Figures 2(a) and (b) show the resulting NIFS spectra.

3. TEMPLATE FITTING EXAMPLES

Assuming that a galaxy spectrum is the convolution of a composite stellar spectrum (combination of all the individual stars present in the local stellar population) with the line-of-sight velocity distribution, the most commonly used method to extract the velocity dispersion from the galaxy spectrum employs a cross-correlation technique using one or more stellar spectra as templates (Tonry & Davis 1979). This technique, however, is sensitive to the effect of template mismatch (e.g., Silge & Gebhardt 2003; Emsellem et al. 2004; Riffel et al. 2008), with the fitting results being affected by the characteristics of the individual stellar spectrum used as template. To obtain a reliable measurement, one should provide the fitting algorithm with a variety of template stellar spectra, which will be internally attributed different fitting weights to obtain the best result.

Silge & Gebhardt (2003) (hereafter SG03) have examined the issue and concluded that it is the equivalent width (EW)—or alternatively, the shape—of the CO band head in the templates that affects the fitting, not the details of the spectral type. Their analysis, using a subsample of stars from the library of Wallace & Hinkle (1997) (hereafter WH97), showed a trend for the velocity dispersion measured for the galaxy to *increase* as the EW of the template star's band head *increases*. They therefore argue that the template sample should span a range of CO EWs, more than simply of spectral types, as the EW of the CO bands is a function of the effective temperature and surface gravity of the star, increasing with decreasing surface gravity or effective temperature.

Figure 3 shows the EW of the first CO overtone (^{12}CO (2–0) at 2.294 μm) in our sample, measured using the IRAF task *onedspec.splot* in the window 2.293–2.322 μm, that is, from the blue edge of the (2–0) band head to the blue edge of the (3–1) band head, plotted as a function of the effective temperature (T_{eff}). This window is larger than the one used by SG03 (2.288–2.305 μm), but avoids trying to define a "continuum" point among the resolved ^{12}CO (2–0) resonance lines. The resulting EWs are about twice the value obtained using SG03 wavelength range. The EWs in the data ranges from less than 5 to over 30 Å. For the template stars not in the sample of Cayrel de Strobel et al. (1997), the value of T_{eff} was obtained from Table 15.7 of Allen's Astrophysical Quantities, 4th edition (Allen 2000), using a simple linear interpolation between the two nearest spectral types when necessary. Figure 4 presents a sample of spectra in the spectral range including the Mg I 2.2814 μm line (left), the first CO and part of the second (^{12}CO (3–1) at 2.323 μm) overtones, to illustrate the different EWs and profiles.

As an example of the use of the templates, we selected actual data from three Gemini programs, GS-2005B-Q-65, a GNIRS/IFU+111 line mm^{-1} observation of the Seyfert galaxy NGC 7582, centered at 2.24 μm (Riffel et al. 2009); GN-2006A-SV-123; and GN-2007A-Q-25, NIFS observations of the Seyfert galaxies NGC 4051, and NGC 4258, respectively (Riffel et al. 2008; R. A. Riffel et al. 2010, in preparation). The analysis technique used was the penalized pixel fitting (pPXF) method of Cappellari & Emsellem (2004), which allows the use of one or several template stellar spectra, and to vary the weights

of the contribution of the different templates to obtain the best fit. A complete description of the data, reduction procedure, and analysis is presented in the first two references above.

Figures 5 and 6 present full two-dimensional velocity dispersion maps for NGC 4051 and NGC 7582 respectively, using a single star with smaller (HD 105028) and larger (HD 30354) CO EWs, and the full library. Sample spectra and corresponding fits, extracted from the data cubes, are show in Figure 7. The effect is quite evident: the large-scale structures in the maps are similar for all stars, but the structures in smaller scales and the mean σ values vary significantly, with *larger* EWs in the templates resulting in *lower* velocity dispersion values measured from the galaxy spectra.

This is the opposite result found by SG03 and prompted a more detailed analysis of the assumed dependency of the fitting result with the stellar template characteristics. To start with, we repeated the fitting of the NGC 4051 off-nucleus spectrum show in Figure 7, using each individual template star in the present library. The galaxy spectrum was then degraded in resolution and the fitting process repeated using each of the stars in the WH97 library with detectable CO absorption (63 objects in total). Since the velocity dispersion of NGC 4051 is quite low, and the resolution of the WH97 templates is $R \sim 3000$, we repeated the same process for the nuclear spectrum of NGC 4258, which has $\sigma \sim 170$ km s^{-1}, closer to that of the object analyzed by SG03. The results are shown in Figure 8. The fitting results using our templates are shown as filled squares; the open triangles are the results from the fitting using the stars from WH97. An average error of 8 km s^{-1} is assumed (estimated by Riffel et al. 2008 from the fitting of the NGC 4051 datacube). The dotted lines indicate the value of σ obtained by fitting the galaxies using all stars from our library simultaneously.

The top panel, with the results for the NGC 4258 nuclear spectrum, gives an indication of why we see a different trend from SG03. Those authors selected only nine stars from the WH97 library, and the dependence found with EW rests strongly in the σ value obtained from the template at the lower end of the EW range (see their Figure 4, remembering that the EW plotted here are about a factor of 2 larger due to the different window used in the measurement). The scattering of points for the stars with EW < 10 Å would indicate that, had they chosen another star, they would have perhaps found a very weak to no dependence of σ on EW, or even a negative correlation as the NGC 4051 fitting seems to indicate.

For this later galaxy, the low dispersion velocity coupled with the lower resolution of the WH97 create a quite distinct negative correlation, with σ *decreasing* as the EW increases. Looking at the results using our higher resolution templates, this correlation is much weaker, and essentially rests—just as before—in the one or two templates at the lower end of the EW range. Therefore, the only systematic effect we can derive from our plots is that for templates with lower EW to overestimate the σ in the galaxy spectrum when such velocity dispersion is already low and close to the limits allowed by the spectral resolution of the data and templates.

We are, therefore, led to conclude that the resulting velocity dispersion is not directly dependent on the EW of the CO band in the template star, just as SG03 concluded that it was not directly dependent on its spectral type. For NGC 4258, the two K0 III stars in our library result in σ values more than 60 km s^{-1} apart, but at the same time it can be seen in the top panel of Figure 8 that templates with essentially the same EW of around 11 Å can yield results ranging from 140 to 240 km s^{-1}.
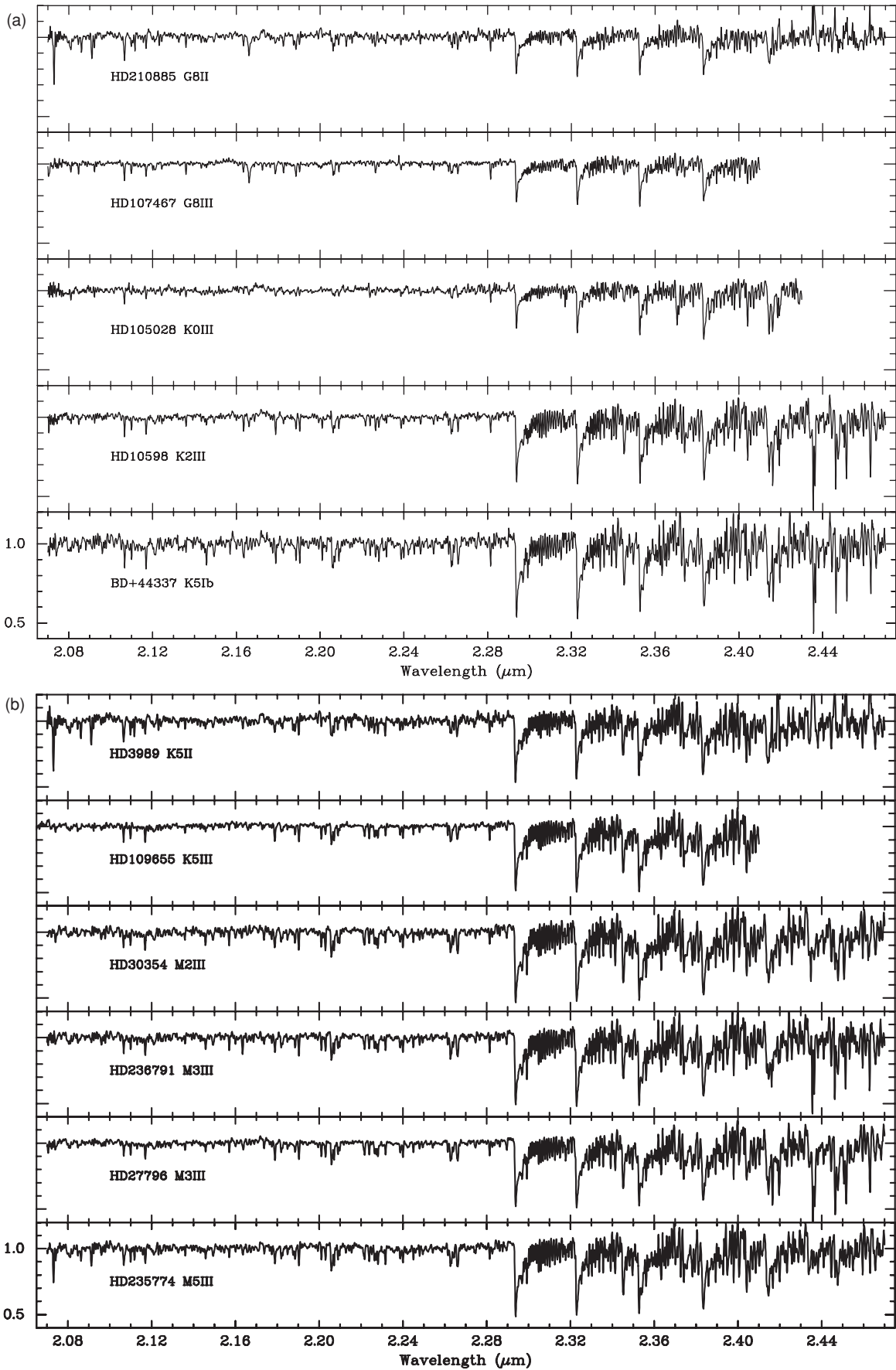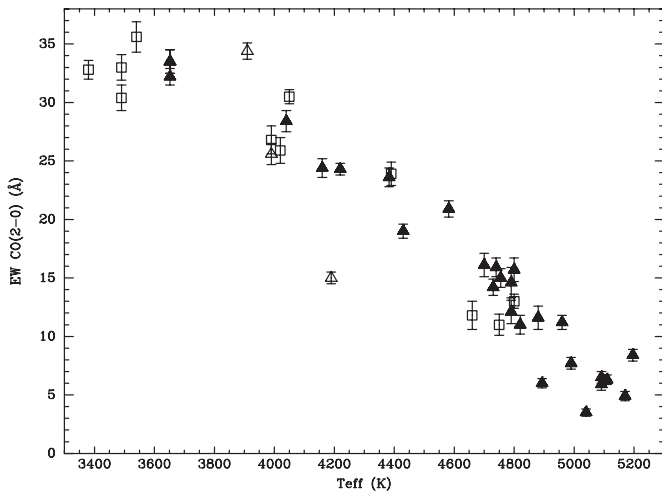
Figure 2. NIFS template spectra, arranged by spectral type.
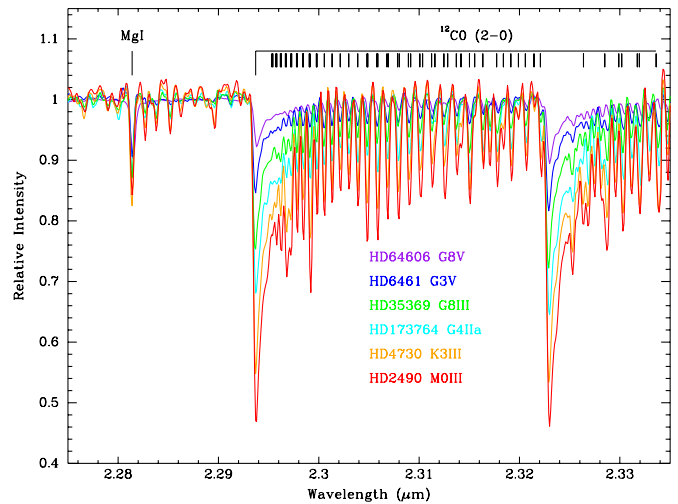
Figure 3. EW of the CO (2–0) 2.294 μm band for our sample, plotted as a function of effective temperature. The EW has been measured in the 2.293–2.322 μm window and the errors correspond to upper and lower placement of the continuum. The GNIRS templates are represented as triangles, the NIFS sample as squares. Closed symbols are stars with temperatures from Cayrel de Strobel et al. (1997), while open symbols correspond to stars for which the temperature was approximated from the spectral type. The star with EW = 15 Å and $T_{\rm eff} \sim 4200$ K is HD 113538 (see note in Table 1).

Figure 4. Sample GNIRS template spectra including the Mg I, the first and part of the second CO overtones, to illustrate the different EWs and profiles. Note how the individual ^{12}CO (2–0) resonance lines are resolved. The CO line identification was taken from the high resolution atlas of Hinkle et al. (1995).

It is more likely that there is not a simple dependence of the fitting result with any particular characteristic of the template star spectrum, but rather that each template, taken in isolation, yields a result that is better or worse, when comparing with the actual σ of the galaxy, depending on how close that individual template is to the overall characteristics of the stellar population contained in the galaxy spectrum. This example illustrates the importance of using a complete stellar library in the determination of the velocity dispersion in galaxies, just as one is needed when analyzing stellar population ages or metallicities in composite spectra.

Figure 9 shows the effect of the slight difference in resolution between the NIFS and GNIRS data. The left panel presents the values of σ measured from all the spectra in the NGC 4051 datacube using only the GNIRS stars as templates against the same measurements using only the NIFS stars. There is an excellent correlation between the two values, but with a systematic

offset to lower σ values using the GNIRS templates. If we consider only the nominal resolving power of the respective gratings, there is a ~ 5.9 km s^{-1} difference in resolution between the two instruments at 2.3 μm. The right panel presents the values obtained for σ after degrading the resolution of the GNIRS templates to the nominal resolving power of the NIFS grating. The 8 km^{-1} error bars in the top left corner correspond to the composite error derived by Riffel et al. (2008). The residual tendency for the NIFS data to overestimate the value of σ at low values can be traced to the uneven distribution of template characteristics of the two samples (the NIFS templates, being fewer and concentrated towards K5 III types or later, do not by themselves provide a full enough representation of the stellar population of the galaxy).
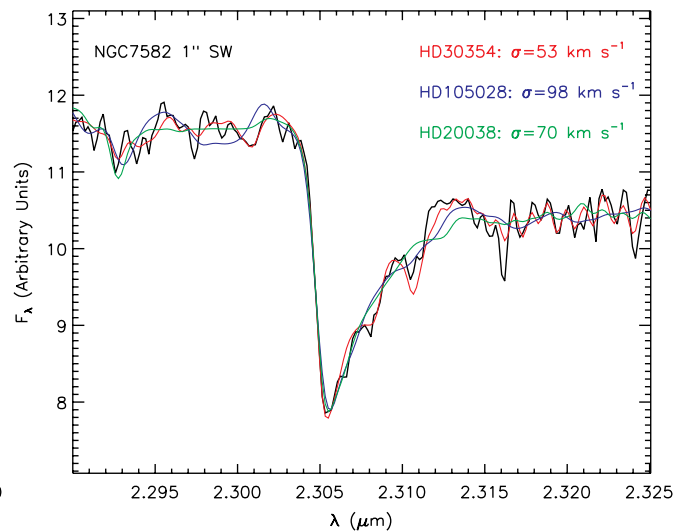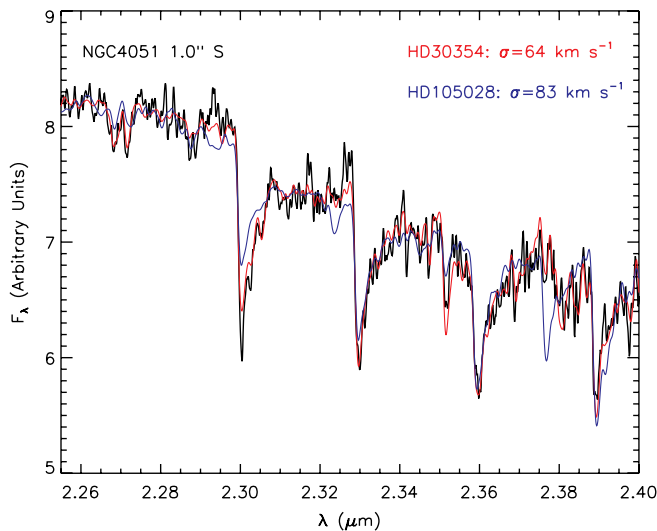
The individual template spectra also show a range of spectral resolution as measured from the FWHM of the arc lines. The resolution of the NIFS templates ranges from 3.12 to 3.26 Å, while that of the GNIRS ones ranges from 2.71 to 3.16 Å. When using the templates to fit NIFS and GNIRS data, the difference is
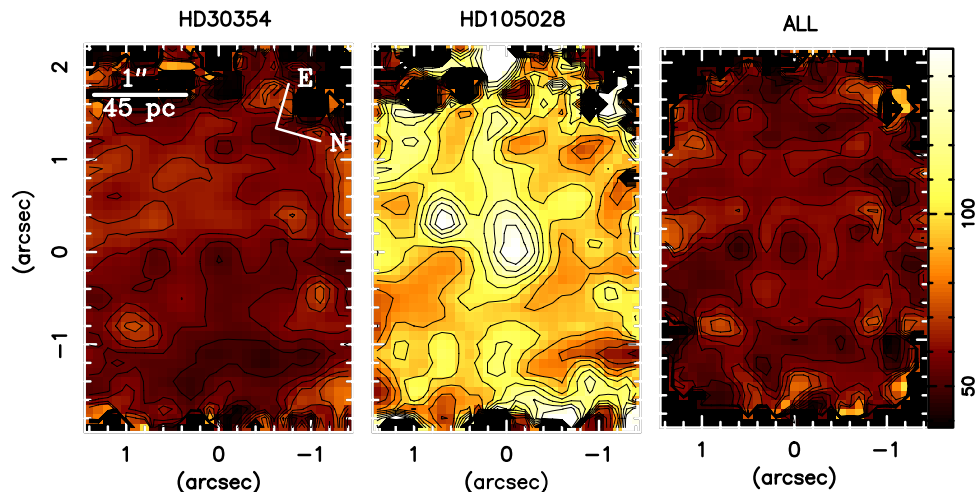
Figure 5. Velocity dispersion maps obtained from NIFS observations of NGC 4051, using as spectral templates for the fitting: (left) only one star, HD 30354 (EW(CO) = 35.6 Å); (middle) only one star, HD 105028 (EW(CO) = 11.8 Å); (right) the full set of templates contained in this library. Not only the derived velocity dispersion values, but also some of the structures in small spatial scales are different in each case.
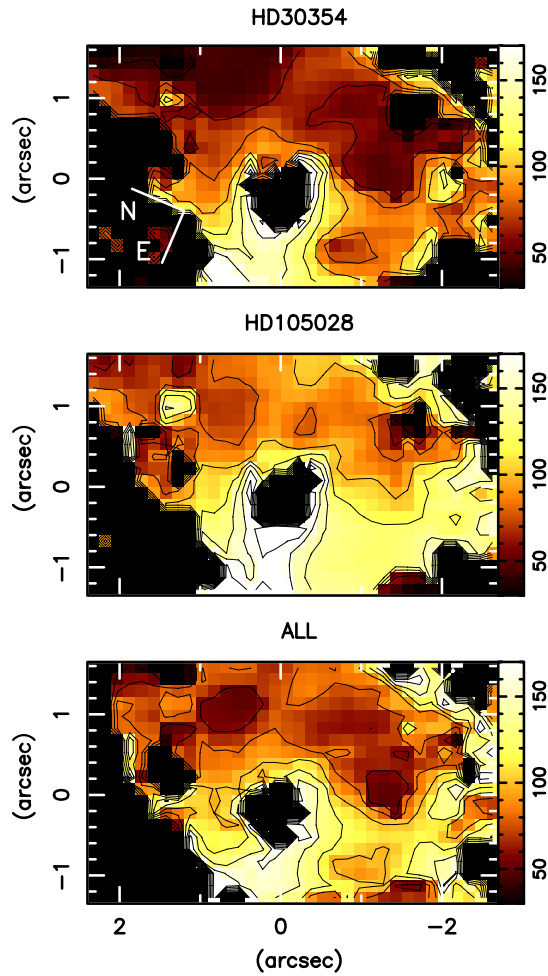
Figure 6. Velocity dispersion maps obtained from GNIRS observations of NGC 7582, using as spectral templates for the fitting: (top) only one star, HD 30354 (EW(CO) = 35.6 Å); (middle) only one star, HD 105028 (EW(CO) = 11.8 Å); (bottom) the full set of templates contained in this library. In this case, the overall structure of the three maps is more similar, but the effect of template mismatch in the resulting values for σ is quite evident.
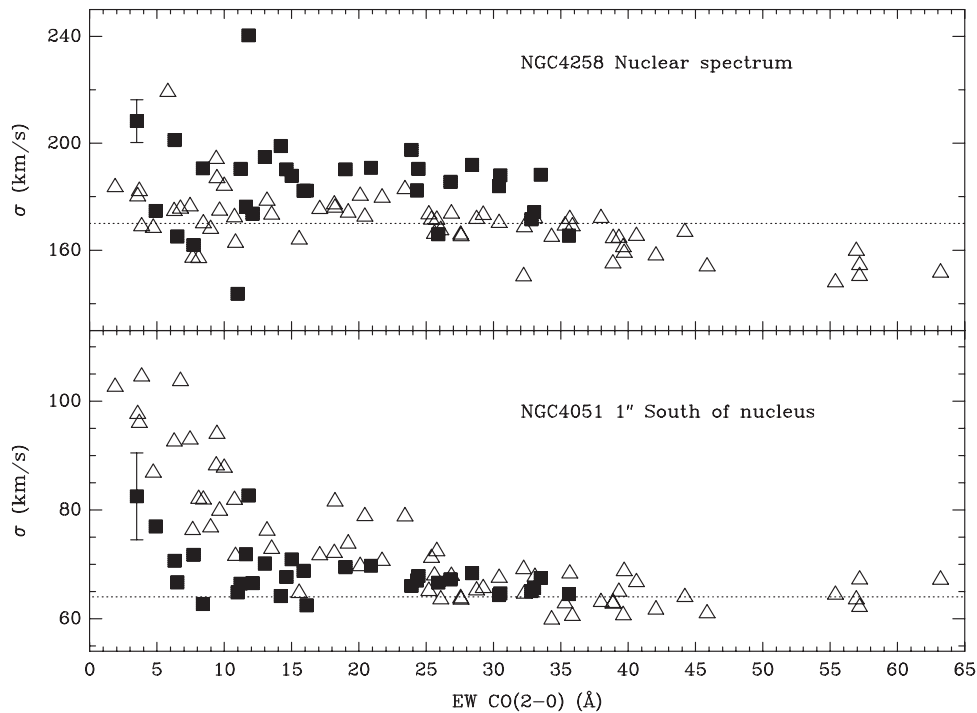
small enough that this effect gets mixed with the noise and fitting errors, but users that require the best precision should convolve each individual spectrum in the library to match the resolution of the data being fitted. Tables 1 and 2 present the resolution of each stellar template, as measured from the arc lines.

One of the most important results that can be obtained from deriving stellar velocity dispersions in the inner regions of active galactic nuclei is the mass of the central supermassive black hole (M_{BH}). The (M_{BH}) versus σ correlation (Gebhardt et al. 2000; Ferrarese & Merrit 2000; Tremaine et al. 2002) can be represented as $\log(M_{BH}/M_\odot) = \alpha + \beta \log(\sigma_*/\sigma_0)$, where $\alpha = 8.13 \pm 0.06$, $\beta = 4.02 \pm 0.32$, and $\sigma_0 = 200$ km s^{-1}. If we take the measurements presented in Figure 5, the value obtained for the bulge central velocity dispersion of the galaxy NGC 4051 using the full library for the fitting is $\sim$60 km s^{-1}, which from the above equation results in $M_{BH} \sim 1.1 \times 10^6\ M_\odot$. On the other hand, if only the star HD 105028 (a K0III, the spectral type most commonly used as template) was available for this analysis, the result would be a velocity dispersion of $\sim$105 km s^{-1}, and thus $M_{BH} \sim 1 \times 10^7\ M_\odot$, a full order of magnitude difference!

It is not directly obtainable from the analysis done here if the effect of using the same single stellar template to determine the velocity dispersion in a sample of objects will be a systematic over- or under-evaluation of σ. It may be an effect proportional to the actual value of the velocity dispersion, or even a pure scattering of the points around the actual values, depending on how close a representation of the local stellar population is to the chosen stellar template. In any case, if the mass of the supermassive black hole for a certain object or sample of objects is determined by other methods, while the value of σ is measured by template fitting, the effect of template mismatch can introduce further scattering on the data points in the M_{BH}–σ correlation.

It is, in any case, quite evident that the improvements in the quality of the data sets and in the analysis methods have led studies of stellar velocity dispersion fitting in external galaxies to join the ranks of the more general issue of composite stellar population analysis, in the sense that a well-known, as complete as possible, template base is needed.

Figure 7. Example of the template fitting results for spectra extracted from the data cubes shown in Figures 5 and 6. (left) Spectrum of a region located 1″ South of the nucleus of NGC 4051 (black), with the convolved HD 30354 (red) and HD 105028 (blue) templates overplotted. The resulting value of σ for each fit is shown in the top right corner. (right) Same as previous, for the spectrum of a region located 1″ South-West of the nucleus of NGC 7582, with the addition of the fit using HD 20038 (EW(CO) = 8.4 Å) as template (green).

Figure 8. Velocity dispersion resulting from fitting individual template stars from this library (filled squares) and that of Wallace & Hinkle (1997) (open triangles), plotted as a function of the EW of the ^{12}CO (2–0) absorption band. The top panel presents the results for the nuclear spectrum of NGC 4258, the bottom panel for an off-nuclear spectrum in NGC 4051. The dashed line is the velocity dispersion value found by using all the stars in the present library as initial input to the fitting program. The error bar corresponds to an average error of 8 km s^{-1}; individual errors tend to be slightly larger (10–12 km s^{-1}) for low EW templates fitting a low σ spectrum such as NGC 4051, or slightly smaller for larger template EW and σ.
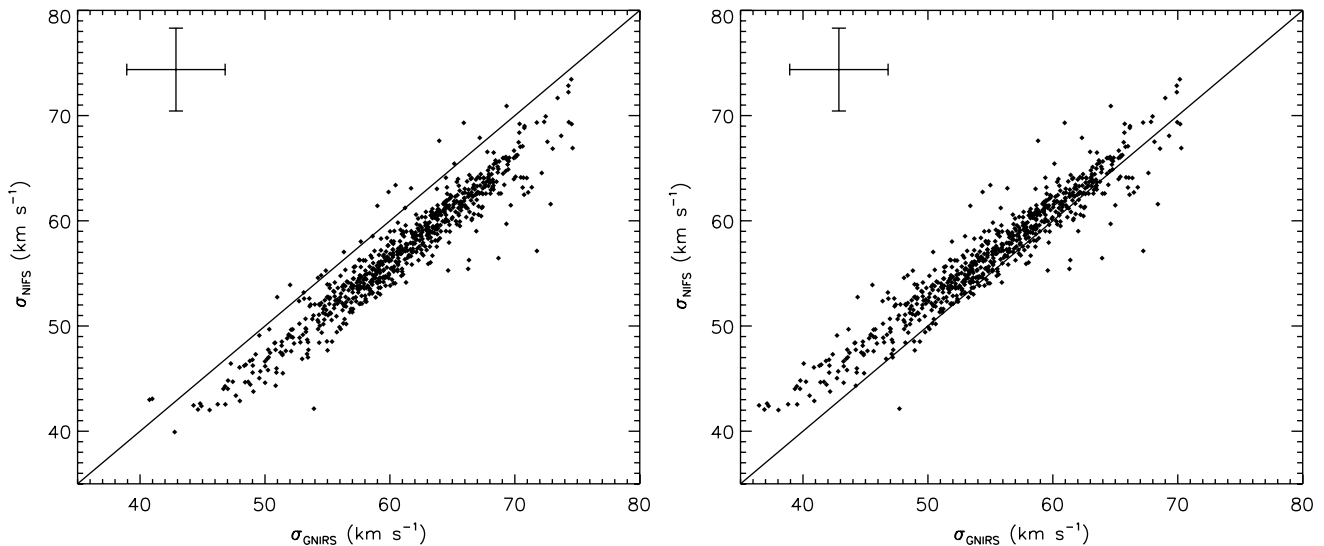
Figure 9. Correlation between the velocity dispersion measured from the NGC 4051 datacube using only the stellar templates from the GNIRS sample [σ(GNIRS)] and from the NIFS sample [σ(NIFS)]. The left panel shows the result using the templates in their native resolution, while in the right panel the resolution of the GNIRS templates was degraded to match the nominal resolution of the NIFS grating.

4. AVAILABILITY OF THE LIBRARY

The Gemini library of late-type stellar templates can be downloaded from the Gemini Web site as individual objects or in two compressed files for the NIFS and GNIRS stars: http://www.gemini.edu/sciops/instruments/nearir-resources/?q=node/10167.

The page contains links to the final processed spectra and details of the data reduction. It also presents the history and release notes for the different versions of the library. The version described in this paper corresponds to V1.5 from 2009 January 31.

The data are presented in standard FITS format, and the user can select either the GNIRS "red" (2.24–2.42 μm) or "blue" (2.15–2.32 μm) spectral ranges at their native spectral binning or the combined spectrum (when both ranges were observed), rebinned to 1 Å pixel^{-1}. The NIFS spectra are also presented at native binning and rebinned to 1 Å pixel^{-1}. All data were kept

with their original spectral resolution, so the users can more adequately adjust the templates to the actual resolution of their own data sets.

The community at large is welcome to download all or part of the library as needed, and users of GNIRS and NIFS are encouraged to explore its use as an alternative to requesting further observation of spectral standards with their science programs. All the GNIRS data collected under program GS-2006B-DD-3 has been made public from the start in the Gemini Science Archive. The NIFS data were subject to the standard proprietary period. If the raw data are re-processed to be used in papers or publications, please use the standard Gemini acknowledgment text for archival data and the appropriate program IDs.

REFERENCES

Allington-Smith, J. R., Content, R., Dubbeldam, C. M., Robertson, D. J., & Preuss, W. 2006, MNRAS, 371, 380
Allington-Smith, J., et al. 2007, MNRAS, 376, 785
Barbosa, F. K. B., Storchi-Bergmann, T., Cid Fernandes, R., Winge, C., & Schmitt, H. 2006, MNRAS, 371, 170
Cappellari, M., & Emsellem, E. 2004, PASP, 116, 138
Cappellari, M., Neumayer, N., Reunanen, J., van der Werf, P. P., de Zeeuw, P. T., & Rix, H.-W. 2009, MNRAS, 394, 660
Cappellari, M., et al. 2007, MNRAS, 379, 418
Cayrel de Strobel, G., Soubiran, C., Friel, E. D., Ralite, N., & Francois, P. 1997, A&AS, 124, 299
Cox, A. (ed.) 2000, Allen's Astrophysical Quantities (4th ed.; New York: Springer)
Dumas, G., Mundell, C. G., Emsellem, E., & Nagar, N. M. 2007, MNRAS, 379, 1249
Elias, J. H., et al. 1998, Proc. SPIE, 3354, 555
Emsellem, E., Greusard, D., Combes, F., Friedli, D., Leon, S., Pécontal, E., & Wozniak, H. 2001, A&A, 368, 52
Emsellem, E., et al. 2004, MNRAS, 352, 721
Ferrarese, L., & Merrit, D. 2000, ApJ, 539, L9
Förster Schreiber, N. M. 2000, AJ, 120, 2089
Ganda, K., Falcón-Barroso, J., Peletier, R. F., Cappellari, M., Emsellem, E., McDermid, R. M., de Zeeuw, P. T., & Carollo, C. M. 2006, MNRAS, 367, 46
Gebhardt, K., et al. 2000, ApJ, 539, L13
Gray, R. O., Corbally, C. J., Garrison, R. F., McFadden, M. T., Bubar, E. J., McGahee, C. E., O'Donoghue, A. A., & Knox, E. R. 2006, AJ, 132, 161
Hinkle, K., Wallace, L., & Livingston, W. 1995, PASP, 107, 1042
Ivanov, V. D., Rieke, M. J., Engelbracht, C. W., Alonso-Herrero, A., Rieke, G. H., & Luhman, K. L. 2004, ApJS, 151, 387
Kleinmann, S. G., & Hall, D. N. B. 1986, ApJS, 62, 501
Márquez, I., Masegosa, J., Durret, F., González Delgado, R. M., Moles, M., Maza, J., P'erez, E., & Roth, M. 2003, A&A, 409, 459
McGregor, P. J., et al. 2003, Proc. SPIE, 4841, 1581
Ramirez, S. V., Depoy, D. L., Frogel, J. A., Sellgren, K., & Blum, R. D. 1997, AJ, 113, 1411
Riffel, R. A., Storchi-Bergmann, T., Dors, O. L., & Winge, C. 2009, MNRAS, 393, 783
Riffel, R. A., Storchi-Bergmann, T., Winge, C., McGregor, P. J., Beck, T., & Schmitt, H. 2008, MNRAS, 385, 1129
Silge, J., & Gebhardt, K. 2003, AJ, 125, 2809
Tonry, J., & Davis, M. 1979, AJ, 84, 1511
Tremaine, S., et al. 2002, ApJ, 574, 740
Wallace, L., & Hinkle, K. 1997, ApJS, 111, 445